Sustainable Biodiesel Synthesis from Cherry Seed Kernels via Electrochemical Transesterification

Claudia Cirillo[a], Mariagrazia Iuliano[b], Faraz Khan[c], Giorgio Crescenzo[d] and Maria Sarno[e]

[a]Department of Physics "E.R. Caianiello", and NANO_MATES Research Centre, University of Salerno, via Giovanni Paolo II, 132 - 84084 Fisciano (SA), Italy, e-mail: clcirillo@unisa.it, CA
[b]Department of Physics "E.R. Caianiello", and NANO_MATES Research Centre, University of Salerno, via Giovanni Paolo II, 132 - 84084 Fisciano (SA), Italy, e-mail: maiuliano@unisa.it
[c]Department of Physics "E.R. Caianiello", University of Salerno, via Giovanni Paolo II, 132 - 84084 Fisciano (SA), Italy, e-mail: fkhan@unisa.it
[d]Department of Physics "E.R. Caianiello",University of Salerno, via Giovanni Paolo II, 132 - 84084 Fisciano (SA), Italy, e-mail: gcrescenzo@unisa.it
[e]Department of Physics "E.R. Caianiello", and NANO_MATES Research Centre, University of Salerno, via Giovanni Paolo II, 132 - 84084 Fisciano (SA), Italy, e-mail: msarno@unisa.it

Abstract:
The current global dependence on non-renewable energy sources, which account for about 35% of the global energy mix, has led to increased greenhouse gas emissions and global warming. In this context, biodiesel represents a sustainable alternative to conventional fossil fuels, being a renewable and biodegradable fuel with a lower pollutant emission profile. Biodiesel can be produced from various organic feedstocks, including non-edible sources such as waste oils and seed-derived oils. Among these, oil extracted from sweet cherry seed kernels (SCK) represents a promising resource, as the industrial processing of sweet cherries generates large amounts of waste and the seeds contain up to 32–36% oil. In this study, biodiesel production from sweet cherry seed kernel oil (SCKO) was investigated using an electrochemical transesterification process. This technique is based on the application of a voltage in an electrolytic cell, where the generation of OH^- ions promotes the reaction between oil and alcohol, potentially reducing energy demand and environmental impact. To improve reaction efficiency, a CaO/Fe_3O_4@MWCNTs heterogeneous nanocatalyst was synthesized and employed, combining high catalytic activity, stability, and easy magnetic separation. The results demonstrate that the developed CaO/Fe_3O_4@MWCNTs catalyst enables efficient conversion of SCKO into biodiesel, achieving a maximum yield of 98.15% under optimal conditions (30 V, 2 wt.% NaCl, 3 h). This approach provides new insights into the sustainable production of biofuels from renewable and non-edible sources.

Keywords: sweet cherry seed kernel oil; biodiesel; electrochemical transesterification; CaO/Fe_3O_4@MWCNTs nanocatalyst**.**

1 Introduction

The global demand for sustainable energy is continuously increasing due to rapid population growth, rising petroleum prices, depletion of fossil fuel resources, and governmental policies aimed at reducing environmental pollution through the promotion of renewable energy sources [1,2]. In this context, biodiesel represents a promising alternative to conventional diesel fuel. It is a renewable biofuel composed of monoalkyl esters of long-chain fatty acids and can be used in diesel engines without significant modifications [3,4]. Moreover, biodiesel is biodegradable, non-toxic, and exhibits a more favourable emission profile compared to petroleum-based diesel [5,6]. One of the major challenges in biodiesel production is the cost of feedstock, which can account for approximately 70–95% of the total production cost [7]. The use of edible oils has raised concerns related to the food versus fuel debate, prompting the exploration of alternative feedstocks such as waste cooking oils, animal fats, non-edible oils, and algal oils [8-10]. Recently, increasing attention has been directed toward oils derived from seeds and kernels of fruits belonging to the Rosaceae family, including plum, apricot, pear, and cherry [11,12]. These materials are byproducts of the food industry and therefore represent low-cost and sustainable feedstocks. Among them, sweet cherry kernel oil (SCKO) has attracted particular interest due to its high content of unsaturated fatty acids, mainly oleic and linoleic acids [11]. Additionally,

SCKO contains valuable bioactive compounds such as tocopherols, sterols, and carotenoids, which enhance its potential for various applications [11,13,14]. However, previous studies have indicated that SCKO is not suitable for direct human consumption, suggesting its potential utilization in energy-related applications such as biodiesel production. The valorization of such agro-industrial residues aligns with the principles of circular bioeconomy and sustainable resource management. So far, biodiesel production from SCKO has primarily been investigated using homogeneous catalysts (e.g., KOH) and assisted techniques such as ultrasound and microwave irradiation [15,16]. However, homogeneous catalytic systems suffer from several drawbacks, including difficult product separation, soap formation, and environmental concerns. In contrast, heterogeneous catalysts offer significant advantages, such as ease of separation, reusability, and reduced environmental impact. Among heterogeneous catalysts, calcium oxide (CaO) is widely recognized for its excellent catalytic performance, including strong basicity, low cost, high stability, non-corrosive nature, and availability from natural and waste sources. CaO has been successfully applied in the transesterification of various oils. Nevertheless, its catalytic performance can be further enhanced through nanostructuring. In particular, the incorporation of CaO with magnetic materials such as Fe_3O_4 and high-surface-area supports like multi-walled carbon nanotubes (MWCNTs) enables the development of advanced nanocatalysts with improved activity, enhanced stability, and facile magnetic recovery. On the other hand, electrolysis has been increasingly studied for biodiesel production because it is eco-friendly, insensitive to the free fatty acid and water content in oil, and exhibits low energy consumption. In such systems, the application of an electric field promotes the formation of reactive species that accelerate the transesterification reaction [17,18]. This method involves employing an electrochemical system comprising an anode and a cathode. When a voltage is applied to the electrolysis cell of an electrochemical system, electrochemical reactions occur and generate OH^- ions on the cathode side, and these ions facilitate the transesterification of alcohol and oil to produce biodiesel. Based on these considerations, the present study proposes an innovative approach for biodiesel production from sweet cherry seed kernel oil via an electro-assisted process using a CaO/Fe_3O_4@MWCNT nanocatalyst. This system combines the advantages of heterogeneous catalysis with electrochemical activation, leading to enhanced reaction kinetics, improved biodiesel yield, and increased process sustainability. Specifically, the oil was extracted from sweet cherry seed kernels and characterized in terms of fatty acid composition and physicochemical properties. Subsequently, it was converted into biodiesel through nanocatalyst-assisted methanolysis under electrochemical conditions. Finally, the properties of the produced biodiesel were evaluated in accordance with international fuel standards.

2 Materials and Methods

Sweet cherry seed kernels (*Prunus avium*, SCK) were supplied by a cherry jam production facility located in Campania. Ethanol, 2-propanol, hexane, and other reagents were purchased from Aldrich Chemical Co. and used without further purification, all of analytical grade.

2.1 Fabrication of CaO/Fe_3O_4@MWCNTs nanocatalyst

2.1.1 Oxidation of MWCNTs

MWCNTs were oxidized following a modified procedure based on Prlainovic et al. [19]. Briefly, 300 mg of MWCNTs were dispersed in 300 mL of 2.5 M HNO_3 and sonicated for 4 h at 50 °C, with the system maintained in an ice-water bath to control temperature rise. The resulting suspension was filtered and repeatedly washed with deionized water until a neutral pH was reached. The functionalized (o-MWCNTs) were then dried at 80 °C overnight.

2.1.2 Synthesis of Fe_3O_4@MWCNTs

Magnetic nanoparticles based on oxidized multi-walled carbon nanotubes (o-MWCNTs) were synthesized via a solvothermal method [20]. $FeCl_3 \cdot 6H_2O$ was dissolved in 20 mL of ethylene glycol to obtain a homogeneous solution, then o-MWCNTs were added. Subsequently, 3.20 g of NaOH was gradually introduced under vigorous stirring, and the mixture was stirred for 1 h. The resulting suspension was transferred into a Teflon-lined stainless-steel autoclave and heated at 200 °C for 3 h. After cooling to room temperature, the black magnetic product was collected using a magnet, washed several times with deionized water and ethanol, and dried at 60 °C overnight.

2.1.3 CaO deposition on Fe_3O_4@MWCNTs

The CaO/Fe_3O_4@MWCNTs nanocatalyst was prepared by wet impregnation [21]. CaO (7.5 g) was dispersed in 250 mL of distilled water under continuous stirring until a homogeneous suspension was obtained.

Subsequently, Fe_3O_4@o-MWCNTs (1.0 g) were added, and the mixture was stirred at 70 °C for 4 h at 700 rpm. The resulting slurry was dried at 105 °C for 6 h to remove residual moisture. Finally, the dried material was calcined at 700 °C for 4 h to obtain the final catalyst.

2.2 Extraction of cherry kernel oil

Cold pressing (CP) of cherry seeds was carried out using a screw press. A batch of 6 kg of seeds was processed to extract the oil under operating conditions of 70 °C internal temperature and a rotation speed of 26 Hz. The extraction was performed in a single run. The obtained oil was collected in a tank and allowed to settle to promote the sedimentation of fine solid particles. After several days, the clarified upper layer was sampled, transferred into 250 mL amber glass bottles, filled to the top to minimize oxygen exposure, and stored at 4 °C. The oil yield was determined according to Equation (1):

$$\text{SCKO yield (\%)} = (Mo / M) \times 100 \quad (1)$$

where *Mo* represents the mass of extracted oil (g), and *M* is the mass of dried SCK (g). The obtained SCKO yield was 18.5% (see Figure 1a). The fatty acid composition of SCKO was analyzed by gas chromatography–mass spectrometry (GC–MS) according to the EN 14103 standard, using a Thermo Fisher Scientific system equipped with a TraceGOLD™ TG-Polar capillary column (60 m × 0.25 mm × 0.25 µm). The injector and detector temperatures were set at 250 °C, and helium was used as the carrier gas. The oven temperature was programmed from 120 °C to 170 °C at 6.5 °C/min, followed by an increase to 250 °C at 2.75 °C/min. Prior to analysis, samples were derivatized using the BF_3–methanol method, and FAMEs were identified by comparison with a C14–C24 standard mixture. The fatty acid profile is reported in Table 1, showing that C18:2 is the predominant component, followed by C18:1, C16:0, and C18:3. ^{1}H NMR spectra of SCKO were recorded using a Bruker Avance 400 spectrometer operating at 400 MHz. Deuterated chloroform ($CDCl_3$) was used as solvent. For analysis, 10 µL of the sample was dissolved in 500 µL of $CDCl_3$, and the resulting solution was used for spectral acquisition.

Table 1. *Physicochemical properties of SCKO. Values are expressed as mean ± standard deviation (n = 3).*

Property	Unit	Value
Acid value	mgKOH/g	0.08±0.013
Free fatty acid content	%	0.056±0.003
Moisture	%	0.11±0.02
Palmitic acid (C16:0)	wt./wt.%	6.04±1.4
Oleic acid (C18:1)	wt./wt.%	29.35±1.7
Linoleic acid (C18:2)	wt./wt.%	60.40±2.4
Linolenic acid (C18:3)	wt./wt.%	0.21±0.11
Unidentified	wt./wt.%	4.0±1.4

The ^{1}H NMR spectrum of the SCKO (see Figure 1b) show signals in the 0-5.5 ppm range, attributable to the fatty acid component of the oil composition.

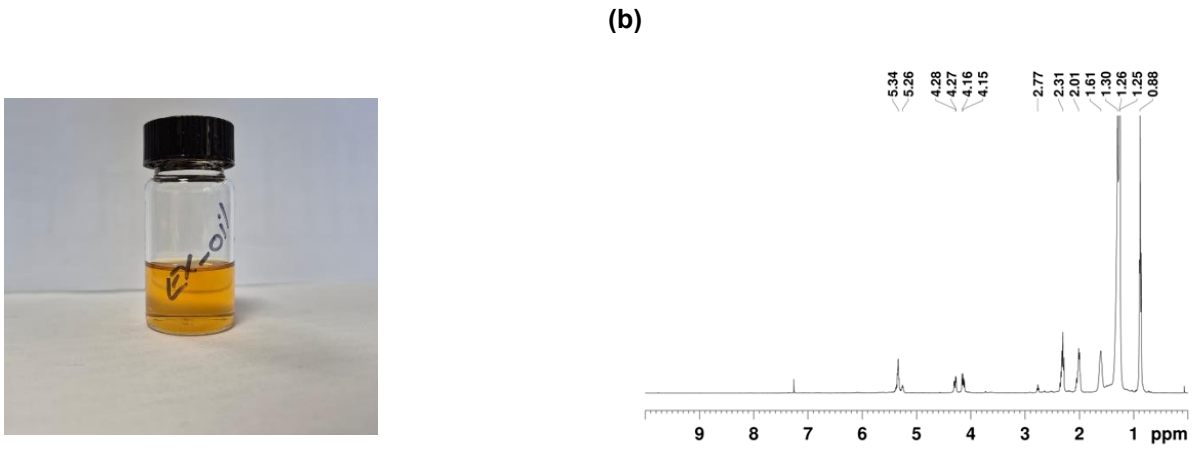

Figure 1*. Photograph of the extracted oil (a), and 1 H NMR spectra of a representative SCKO sample (b).*

The main contributions arise from methylene protons (−CH_2−) of the acyl chains (0.8–2.2 ppm). Signals at 5.34–5.26 ppm are attributed to olefinic protons (–CH=CH–), while signals around 4.1–4.3 ppm correspond to glyceridic protons of triacylglycerols, respectively, in agreement with Table 2. The higher-resolution 400 MHz spectrum allows identification of eight distinct proton signals, consistent with the assignments reported in Table 2.

***Table 2**. Chemical Shifts (δ in ppm) and Assignment of the Signals in the 1 H NMR Spectrum of an SCKO Sample Recorded at 400 MHz.*

δ (ppm)	Proton Group	Assignment
5.34 – 5.26	−CH=CH−	All unsaturated fatty acids
4.28 – 4.15	CH_2−OCOR	Triacylglycerols
2.77	CH=CH−CH_2−CH=CH	Linoleic and linolenic chains
2.31	CH_2−COOH	All acyl chains
2.01	CH_2−CH=CH	All unsaturated fatty acids
1.61	CH_2−CH_2−COOH	All acyl chains
1.30-1.25	−(CH_2) –	All acyl chains
0.88	CH_2−CH_2−CH_2−CH_3	All acyl chains (except linolenyl)

2.3 Synthesis of biodiesel

The electrochemical system consisted of a two-electrode cell equipped with graphite plates serving as both the anode and cathode, connected to a DC power supply (Figure 2).

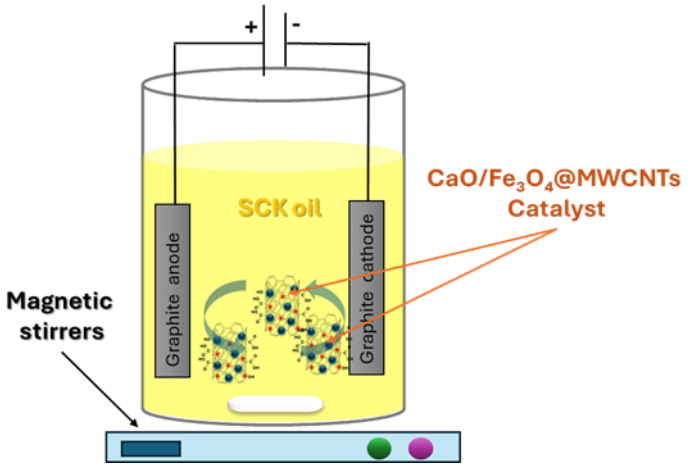

***Figure 2.** Electrolytic setup for the conversion of SCKO into FAME using the CaO/Fe_3O_4@MWCNTs catalyst.*

The CaO/Fe_3O_4@MWCNTs catalyst was directly dispersed in the reaction medium, while continuous magnetic stirring ensured homogeneous mixing and efficient mass transfer. All experiments were performed under the operating conditions reported in Table 3, where the main parameters were systematically varied to evaluate their effect on biodiesel yield. The electrolysis cell consisted of 50 mL of reaction mixture with an oil-to-methanol molar ratio of 1:30, water (2 wt.% with respect to oil), and NaCl as a supporting electrolyte. To enhance the electrical conductivity, NaCl was first dissolved in the methanol–water mixture prior to the addition of the oil, promoting ionic dissociation and facilitating charge transport within the system. Upon application of an electric field, electron flow between the electrodes induces the activation of reactant species and improves interfacial mass transfer. In the presence of the dispersed catalyst, methoxide ions (CH_3O^-) are generated in situ and act as the key reactive species, attacking the carbonyl groups of triglycerides and enabling simultaneous transesterification and esterification reactions. In addition, this study aimed to analyze the influence of key electrochemical parameters, namely applied voltage (V), NaCl concentration (wt.% with respect to oil), and electrolysis time (h) on biodiesel synthesis. Statistical analysis of the experimental data was carried out using Minitab 19, including graphical evaluation and regression modelling. Analysis of variance (ANOVA) was employed to assess the statistical significance of individual factors and their interaction effects on yield (%), based on F- and p-values.

Table 3. *Experimental variables and investigated ranges*

Variable	Range
Voltage (V)	20 ÷30
NaCl (wt.% with respect to oil)	0.5 ÷2.0
Electrolysis time (h)	1 ÷ 3

After completion of the reaction, the biodiesel phase (FAME) was separated from the glycerol layer using a separating funnel and subsequently dried over anhydrous sodium sulfate to remove residual moisture. The biodiesel yield was calculated according to the corresponding equation (2) [22].

$$\text{Yield \%} = (\text{Mass of obtained biodiesel/Mass of SCKO used}) \times 100 \quad (2)$$

^{1}H NMR spectra of the corresponding biodiesel were recorded using a Bruker Avance 400 spectrometer operating at 400 MHz. Deuterated chloroform ($CDCl_3$) was used as solvent. For analysis, 10 µL of the sample was dissolved in 500 µL of $CDCl_3$, and the resulting solution was used for spectral acquisition.

2.4 Characterization

The morphology and elemental composition of the synthesized catalyst were examined by scanning electron microscopy coupled with energy-dispersive X-ray spectroscopy (SEM–EDX, TESCAN VEGA LMH). The crystalline structure was analyzed using X-ray diffraction (XRD) with a Bruker D2 Phaser diffractometer employing CuKα radiation. Thermogravimetric analysis (TGA) was performed on a METTLER TOLEDO TGA-2 instrument under an air atmosphere, with a heating rate of 10 °C/min. Functional groups were identified by Fourier-transform infrared spectroscopy (FT-IR) using a Thermo Scientific Nicolet iS50 spectrometer equipped with a diamond ATR accessory, recorded over the range of 500–4000 cm^{-1}.

3 Results and Discussion

3.1 Catalyst characterization

Figure 3 schematically illustrates the stepwise fabrication of the CaO/Fe_3O_4@MWCNTs nanocatalyst. In the first stage, pristine MWCNTs were treated with 2.5 M HNO_3 to introduce oxygen-containing functional groups such as –COOH and –OH onto their surface. This oxidation step enhances the hydrophilicity and dispersion of nanotubes while providing active sites for the subsequent anchoring of metal species. In the second step, Fe_3O_4 nanoparticles were successfully grown on the surface of the oxidized MWCNTs via a solvothermal process using $FeCl_3 \cdot 6H_2O$ and NaOH. The formation of Fe_3O_4@MWCNTs is evidenced by the uniform decoration of the nanotube surface with magnetic nanoparticles. As highlighted in the figure, the resulting material exhibits magnetic behavior, allowing for rapid and efficient separation from the reaction medium using an external magnetic field. In the final stage, CaO was deposited onto the Fe_3O_4@MWCNTs through a wet impregnation method, followed by drying and calcination. This step leads to the formation of the CaO/Fe_3O_4@MWCNTs composite, where CaO acts as the active catalytic phase, while Fe_3O_4 ensures magnetic recoverability, and MWCNTs provide a high surface area support.

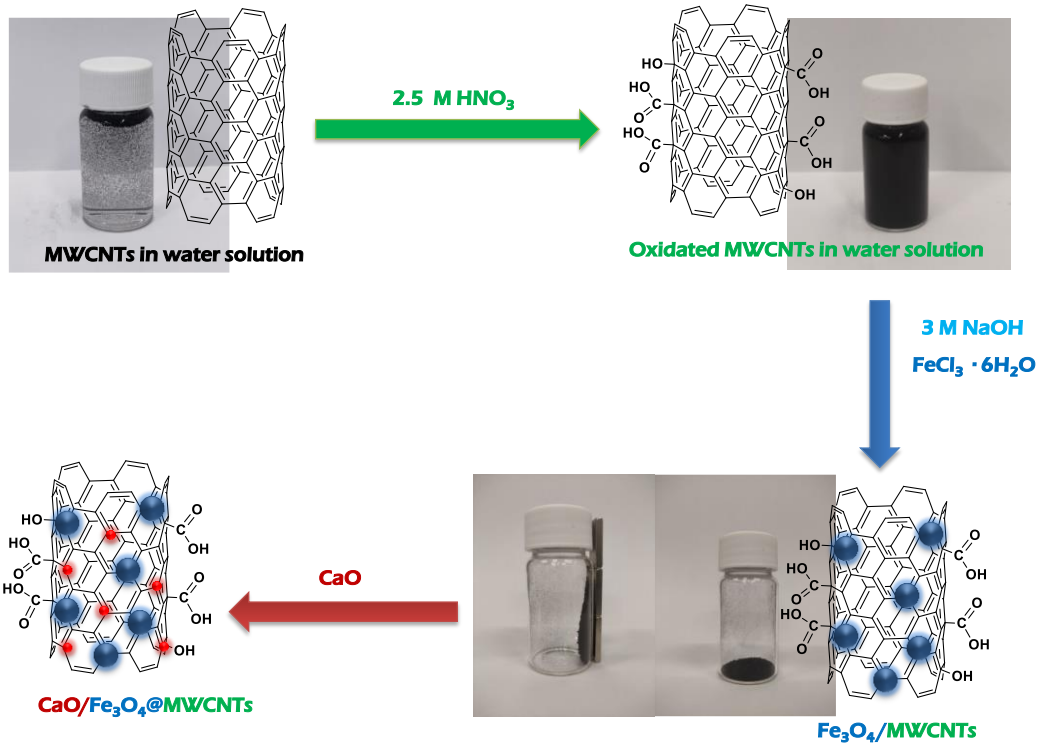

Figure 3. *Schematic illustration of the stepwise synthesis of CaO/Fe_3O_4@MWCNTs nanocatalyst*

The XRD patterns of MWCNTs, Fe_3O_4@MWCNTs, and CaO/Fe_3O_4@MWCNTs are shown in Figure 4. The diffraction peak observed at 2θ ≈ 26° (002) is attributed to the characteristic reflection of MWCNTs [23]. In the Fe_3O_4@MWCNTs sample, three main diffraction peaks appear at 2θ values of 35.2°, 43.1°, and 62.3°, corresponding to the (311), (400), and (440) planes, respectively, which are consistent with the cubic spinel structure of Fe_3O_4 (JCPDS card No. 19-0629). For the CaO/Fe_3O_4@MWCNTs composite, additional diffraction peaks located at 30.5°, 38.6°, and 46.3° are assigned to CaO [24]. The coexistence of these peaks along with those of Fe_3O_4 and MWCNTs confirms the successful synthesis of the composite material.

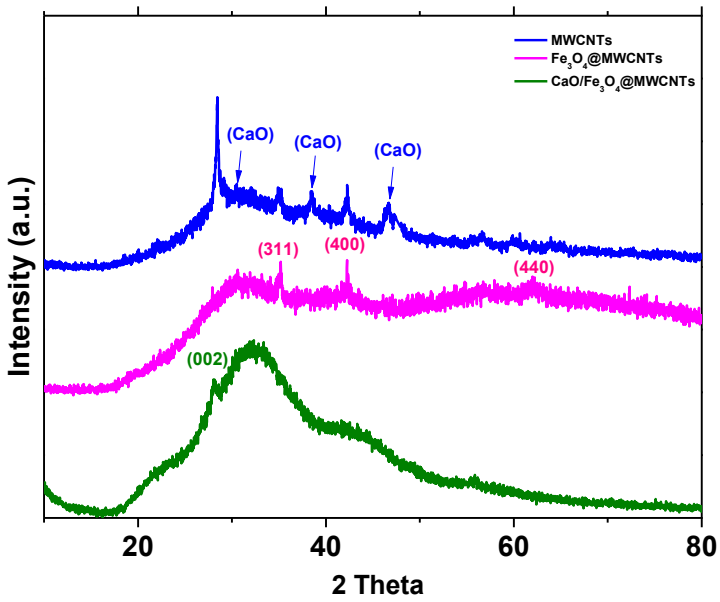

***Figure 4**. XRD patterns of MWCNTs, Fe_3O_4@MWCNTs and CaO/Fe_3O_4@MWCNTs in the 2θ range of 15°-80°.*

The morphology of the materials was investigated by scanning electron microscopy (SEM), and the results are presented in Figure 5. The SEM image of pristine MWCNTs (Figure 5a) shows their typical tubular structure with smooth and entangled surfaces. After Fe_3O_4 deposition (Figure 5b), nanoparticles are observed to be irregularly distributed on the outer walls of the nanotubes, indicating effective anchoring of the magnetic phase onto the MWCNTs. In the CaO/Fe_3O_4@MWCNTs sample (Figure 5c), the surface appears densely covered by particles, resulting in a reduced visibility of the nanotube structure. This suggests a high surface coverage due to the combined presence of Fe_3O_4 and CaO. However, it is not possible to clearly distinguish between the CaO and Fe_3O_4 phases from the SEM images, likely due to their overlapping distribution and nanoscale particle size. Furthermore, the elemental composition of the CaO/Fe_3O_4@MWCNTs catalyst is reported in the corresponding table, confirming the presence of the main elements and thus the successful synthesis of the material. The magnetic behaviour of the Fe_3O_4@MWCNTs sample is illustrated in the inset Figure 5b, demonstrating its effective magnetic response and facilitating its recovery by magnetic separation.

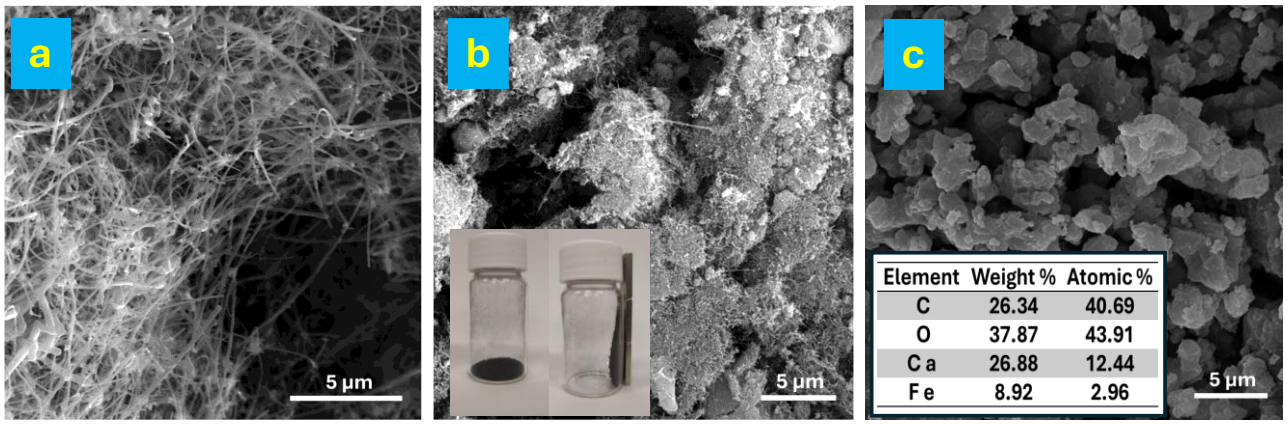

***Figure 5**. SEM micrographs of pristine MWCNTs (a), Fe_3O_4@MWCNTs (b), and CaO/Fe_3O_4@MWCNTs (c) nanocatalyst, with inset (c) showing the corresponding EDX analysis.*

3.2 Analysis of biodiesel synthesis

3.2.1 Model development, evaluation, and verification

The full-factorial design was used to fit the experimental data and to identify the operating conditions that maximize the process yield. In particular, 27 experiments were carried out by investigating the effects of three independent variables, namely Voltage, NaCl concentration, and Time, each evaluated at three levels. The experimental and predicted values of yield are reported in Table 4. The relationship between the response and the operating variables was described by the following regression equation, expressed in terms of the actual variables:

Yield (%) = -69.6 + 2.986 Voltage + 10.68 NaCl + 20.99 Time

The positive coefficients of all three variables indicate that increasing Voltage, NaCl concentration, and Time leads to an increase in yield within the investigated experimental domain. Among the three factors, Time showed the strongest positive effect on the response, followed by NaCl concentration and Voltage, as indicated by the magnitude of the regression coefficients. A comparison between experimental and predicted values showed a generally good agreement, confirming that the model adequately describes the process behavior, despite some deviations in specific runs.

***Table 4.** Experimental matrix for three-level-three-factor response surface analysis*

Run	Voltage (V)	NaCl (wt.% with respect to oil)	Time (h)	Yield (%)	Predicted (%)
1	25	0.5	3	75.14	73.36

2	20	0.5	1	23.56	16.45
3	20	0.5	3	56.12	58.43
4	30	2	2	90.23	83.32
5	30	2	3	98.15	104.31
6	25	2	1	45.61	47.4
7	20	2	1	12.5	32.47
8	20	1.5	3	72.36	69.11
9	25	0.5	2	55.55	52.37
10	30	2	1	60.95	62.33
11	20	2	2	55.15	53.46
12	30	1.5	3	95.15	98.97
13	25	2	2	80.47	68.39
14	30	1.5	1	55.23	56.99
15	20	2	3	64.12	74.45
16	20	0.5	2	40.25	37.44
17	25	1.5	2	75.19	63.05
18	30	1.5	2	85.95	77.98
19	25	1.5	1	50.64	42.06
20	20	1.5	1	21.54	27.13
21	20	1.5	2	53.25	48.12
22	25	2	3	89.57	89.38
23	30	0.5	1	38.45	46.31
24	25	0.5	1	29.57	31.38
25	30	0.5	3	78.16	88.29
26	30	0.5	2	65.28	67.30
27	25	1.5	3	87.15	84.04

The statistical significance of the model and its terms was evaluated by analysis of variance (ANOVA), as reported in Table 5. The results indicate that the regression model is statistically significant, as evidenced by the low p-value ($p < 0.001$). Among the factors investigated, Time showed the most significant effect on the response, followed by NaCl concentration and Voltage. The residual error remained within acceptable limits, confirming that the linear model is suitable for describing the system within the investigated experimental range. No significant lack-of-fit was observed, indicating a good agreement between the model and the experimental data. Within the investigated range, the highest experimental yield was achieved at 30 V, 2 wt.% NaCl, and 3 h, corresponding to 98.15%, while the model predicted 104.31%. Since yields above 100% are not physically meaningful, this result indicates a slight overestimation by the linear regression model near the upper boundary of the design space. Nevertheless, the model remains useful for identifying the optimal region and describing the overall effect of the process variables. This value is comparable to or higher than those reported in the literature for similar feedstocks and catalytic systems, including conventional homogeneous catalysts and CaO-based materials [11,12,21].

Table 5. *Analysis of Variance (ANOVA)*

Source	Degree of Freedom	Sum of Square	Mean Square	F-Value	P-Value
Regression	3	13142	4380.69	73.33	0.000
Voltage	1	4011	4011.09	67.15	0.000
NaCl	1	1198	1198.44	20.06	0.000
Time	1	7933	7932.54	132.79	0.000

Residual Error	23	1374	59.74
Total	26	14516	

R^2 = 0.9054 adj. R^2 = 0.8930, pred. R^2 = 0.8673

3.3 Characterization and properties of biodiesel from SCKO

The GC–MS results (parameter Run 5) of CaO/Fe_3O_4@MWCNTs catalyzed SCKO are presented in Table 6 and indicate the conversion of fatty acids to methyl esters and the separation of glycerol from fatty acids. Further, it was observed that there were no significant deviations in the fatty acid composition of SCKO and biodiesel.

Table 6. GC-MS analysis for determining fatty acid methyl ester compounds.

FAME	Structure	Percentage (wt.%)
Methyl palmitate	$C_{16:0}$	5.99±1.31
Methyl oleate	$C_{18:1}$	29.36±2.21
Methyl linoleate	$C_{18:2}$	59.98±1.24
Methyl linolenate	$C_{18:3}$	0.20±0.07
Unidentified	-	3.75±0.07

The ^{1}HNMR analysis was used to describe the chemical properties of biodiesel produced through the CaO/Fe_3O_4@MWCNTs catalyst. The results of the ^{1}H NMR test are shown in Figure 6. As shown, biodiesel made from SCKO has several parallel peaks. In SCKO biodiesel, a distinct peak is observed at 3.66 ppm, attributed to methyl ester ($–OCH_3$) protons. This signal is absent in the parent oil (see Figure 1b) and confirms the successful conversion to biodiesel. Strong signals are also detected in the range of 1.26–1.35 ppm, corresponding to methylene (CH_2) groups. Additional characteristic peaks appear at approximately 1.60, 2.77, and 5.33–5.37 ppm, which are assigned to β-CH_2, allylic (=CH–CH_2–), and olefinic (–CH=CH–) protons, respectively [25].

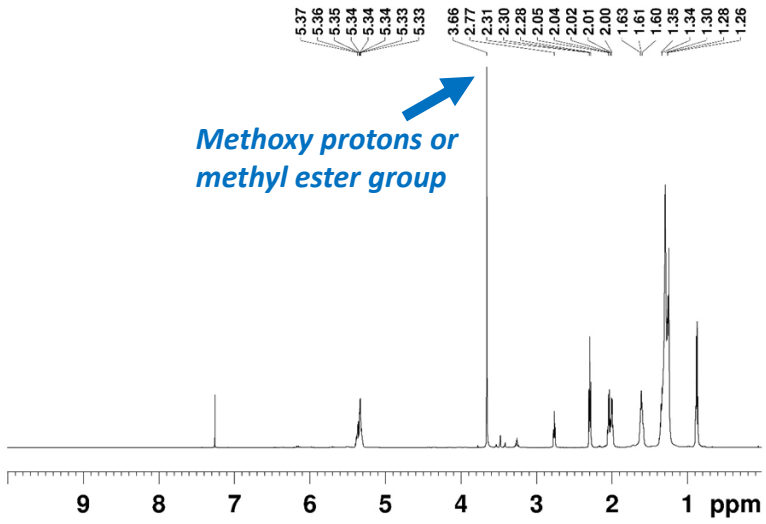

***Figure 6**. ^{1}HNMR spectra of the produced biodiesel from SCKO.*

Figure 7a presents the FT-IR spectra of both the produced biodiesel and the original oil. The biodiesel spectrum exhibits characteristic absorption bands at 1160 cm^{-1} and in the range of 1384-1450 cm^{-1}, which are attributed to ester O-C stretching and asymmetric C-H bending vibrations, respectively. The appearance of these peaks confirms the successful transesterification process and the conversion of SCKO into biodiesel, as these signals are absent in the oil spectrum. In addition, the prominent peak at 1744 cm^{-1} corresponds to the C=O stretching vibration of ester functional groups [26]. Figure 7b illustrates the proposed mechanism of the transesterification reaction catalyzed by CaO/Fe_3O_4@MWCNTs. The reaction begins with the nucleophilic attack of methoxide ions on the carbonyl carbon of triglycerides adsorbed on the catalyst surface, leading to the formation of a

tetrahedral intermediate. This intermediate then rearranges to yield a diglyceride anion and a molecule of methyl ester. The negatively charged intermediate is subsequently stabilized by proton transfer from the catalyst surface, regenerating the active catalytic sites. This sequence repeats for all three ester groups of the triglyceride, ultimately producing one mole of glycerol and three moles of methyl esters [27,28].

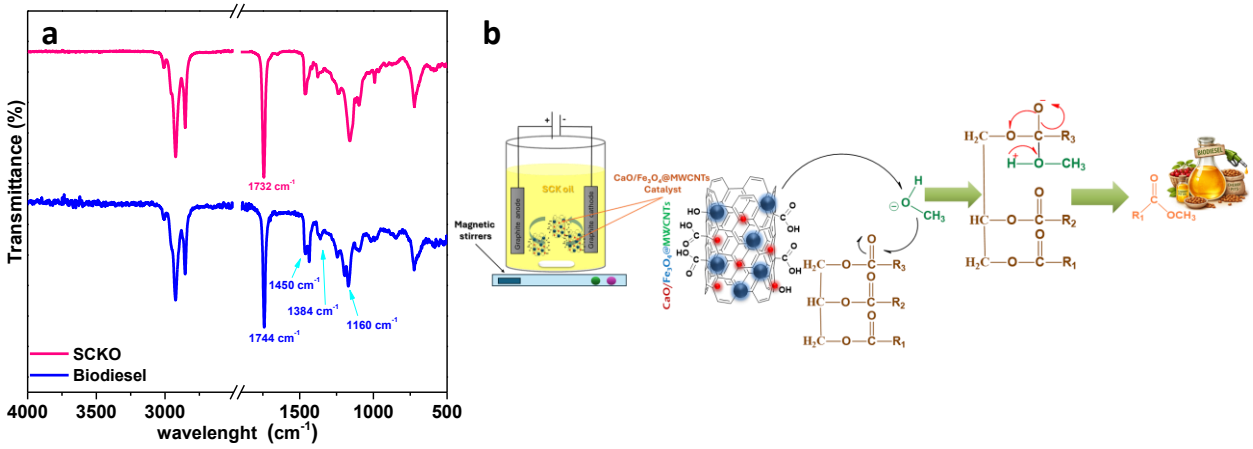

***Figure 7**. FT-IR spectra of the produced biodiesel and the original oil (a); Proposed mechanism of the transesterification reaction catalyzed by CaO/Fe_3O_4@MWCNTs (b).*

The produced SCKO biodiesel exhibited a density of 875 kg/m³ and a kinematic viscosity of 4.24 mm²/s at 40 °C, both complying with the EN 14214 standard requirements. In addition, the higher heating value (HHV), determined using a bomb calorimeter according to ASTM D240, was approximately 39.5 MJ/kg, which is consistent with the values commonly reported for biodiesel derived from vegetable and fruit seed oils. These results confirm the favorable transport and energy properties of SCKO biodiesel for potential renewable fuel applications.

4 Conclusion

This study presents a sustainable and efficient route for biodiesel production from sweet cherry seed kernel oil (SCKO), an abundant agro-industrial waste. The integration of electrochemical transesterification with a CaO/Fe_3O_4@MWCNTs heterogeneous nanocatalyst proved effective in enhancing reaction performance while reducing environmental impact. The developed catalyst exhibited high activity, good stability, and facile magnetic recovery, thereby overcoming the typical limitations associated with homogeneous catalytic systems. The electrochemical approach enabled the in situ generation of reactive species, leading to improved conversion efficiency under relatively mild operating conditions, highlighting its potential for practical application. The highest experimental yield (98.15%) was achieved at 30 V, 2 wt.% NaCl, and 3 h. In addition, statistical analysis highlighted the significant influence of process parameters, particularly reaction time, confirming the effectiveness of the proposed approach for process optimization. Comprehensive characterization (GC–MS, ^{1}H NMR, and FTIR) confirmed the successful conversion of SCKO into biodiesel. The obtained yield is comparable to or higher than those reported in the literature for similar feedstocks and catalytic systems, including conventional homogeneous catalysts and other heterogeneous CaO-based materials.

The proposed approach demonstrates that the combination of waste-derived feedstocks, electrochemical activation, and advanced nanocatalysts represents a promising strategy for the development of efficient and environmentally friendly biodiesel production processes.

References

[1]. Verma, P., & Sharma, M. (2016). Review of process parameters for biodiesel production from different feedstocks. Renewable and Sustainable Energy Reviews, 62, 1063–1071. https://doi.org/10.1016/j.rser.2016.04.054

[2]. Vafaeifard, M., Lee, G., Akib, S., Ibrahim, S., Yoon, Y., & Jang, M. (2016). Facile and economic one-pot synthesis of rigid functional-polyurethane for the effective treatment of heavy metal-contaminated urban storm water run-off. Desalination and Water Treatment, 57(54), 26114–26129. https://doi.org/10.1080/19443994.2016.1164082

[3]. Akhbari, A., Bonakdari, H., & Ebtehaj, I. (2017). Evolutionary prediction of electrocoagulation efficiency and energy consumption probing. Desalination and Water Treatment, 64, 54–63. https://doi.org/10.5004/dwt.2017.20235

[4]. Bonakdari, H., Ebtehaj, I., & Akhbari, A. (2017). Multi-objective evolutionary polynomial regression-based prediction of energy consumption probing. Water Science & Technology, 75(12), 2791–2799. https://doi.org/10.2166/wst.2017.158

[5]. Kulkarni, M. G., & Dalai, A. K. (2006). Waste Cooking OilAn Economical Source for Biodiesel: A Review. Industrial & Engineering Chemistry Research, 45(9), 2901–2913. https://doi.org/10.1021/ie0510526

[6]. Qu, L., Wang, Z., & Zhang, J. (2016). Influence of waste cooking oil biodiesel on oxidation reactivity and nanostructure of particulate matter from diesel engine. Fuel, 181, 389–395. https://doi.org/10.1016/j.fuel.2016.04.113

[7]. Bhuiya, M., Rasul, M., Khan, M., & Ashwath, N. (2020). Biodiesel production and characterisation of poppy (Papaver somniferum L.) seed oil methyl ester as a source of 2nd generation biodiesel feedstock. Industrial Crops and Products, 152, 112493. https://doi.org/10.1016/j.indcrop.2020.112493

[8]. Elouahed, S. K., Asikin-Mijan, N., G, A. A., Kaddour, O., Yusop, Mimoun, H., Samidin, S., Mansir, N., & Taufiq-Yap, Y. (2024). Optimization of the activity of Mo7-Zn3/CaO catalyst in the transesterification of waste cooking oil into sustainable biodiesel via response surface methodology. Energy Conversion and Management, 303, 118185. https://doi.org/10.1016/j.enconman.2024.118185

[9]. Ao, S., Gouda, S. P., Selvaraj, M., Boddula, R., Al-Qahtani, N., Mohan, S., & Rokhum, S. L. (2023). Active sites engineered biomass-carbon as a catalyst for biodiesel production: Process optimization using RSM and life cycle assessment. Energy Conversion and Management, 300, 117956. https://doi.org/10.1016/j.enconman.2023.117956

[10]. Uslu, S., Maki, D. F., & Al-Gburi, A. S. K. (2023). Synthesis of spirulina microalgae biodiesel, and experimental research of its effects on compression ignition engine responses with iron II-III oxide (Fe_3O_4) nanoparticle supplementation. Energy Conversion and Management, 293, 117457. https://doi.org/10.1016/j.enconman.2023.117457

[11]. Demirbas, A. (2016). Biodiesel from kernel oil of sweet cherry (Prunus aviumL.) seed. Energy Sources Part a Recovery Utilization and Environmental Effects, 38(17), 2503–2509. https://doi.org/10.1080/15567036.2015.1091868

[12]. Almasi, S., Najafi, G., Ghobadian, B., & Jalili, S. (2021). Biodiesel production from sour cherry kernel oil as novel feedstock using potassium hydroxide catalyst: Optimization using response surface methodology. Biocatalysis and Agricultural Biotechnology, 35, 102089. https://doi.org/10.1016/j.bcab.2021.102089

[13]. Yılmaz, C., & Gökmen, V. (2013). Compositional characteristics of sour cherry kernel and its oil as influenced by different extraction and roasting conditions. Industrial Crops and Products, 49, 130–135. https://doi.org/10.1016/j.indcrop.2013.04.048

[14]. Kazempour-Samak, M., Rashidi, L., Ghavami, M., Sharifan, A., & Hosseini, F. (2021). Sour Cherry (Cerasus vulgaris Miller) Kernel Oil as the Novel Functional Edible Oil: Sensory Evaluation and Antioxidant and Physicochemical Properties. Journal of Food Quality, 2021, 1–9. https://doi.org/10.1155/2021/5529613

[15]. Nguyen, H. C., Wang, F., Dinh, K. K., Pham, T. T., Juan, H., Nguyen, N. P., Ong, H. C., & Su, C. (2020). Microwave-Assisted noncatalytic esterification of fatty acid for biodiesel production: a Kinetic study. Energies, 13(9), 2167. https://doi.org/10.3390/en13092167

[16]. Islam, M. S., Hart, C. R., & Casadonte, D. (2022). Ultrasound-assisted solid Lewis acid-catalyzed transesterification of Lesquerella fendleri oil for biodiesel synthesis. Ultrasonics Sonochemistry, 88, 106082. https://doi.org/10.1016/j.ultsonch.2022.106082

[17]. Helmi, M., Hemmati, A., & Tahvildari, K. (2022). Production of biodiesel from salvia mirzayanii oil via electrolysis using KOH/Clinoptilolite as catalyst. Journal of Environmental Health Science and Engineering, 20(1), 187–204. https://doi.org/10.1007/s40201-021-00766-y

[18]. Khan, F., Adami, R., Iuliano, M., Cirillo, C., Gallucci, L., & Sarno, M. (2025b). Low-cost and sustainable electrocatalytic approach for the direct synthesis of biodiesel from waste cooking oil. Biomass and Bioenergy, 206, 108684. https://doi.org/10.1016/j.biombioe.2025.108684

[19]. Prlainović, N. Ž., Bezbradica, D. I., Rogan, J. R., Uskoković, P. S., Mijin, D. Ž., & Marinković, A. D. (2016). Surface functionalization of oxidized multi-walled carbon nanotubes: Candida rugosa lipase immobilization. Comptes Rendus Chimie, 19(3), 363–370. https://doi.org/10.1016/j.crci.2015.10.008

[20]. Iuliano, M., Cirillo, C., Astorga, E. N., & Sarno, M. (2024). A new nanocomposite as adsorbent and catalyst for enhanced removal of methylene blue. Surfaces and Interfaces, 51, 104582. https://doi.org/10.1016/j.surfin.2024.104582

[21]. Widayat, Satriadi, H., Setyojati, P. W., Shihab, D., Buchori, L., Hadiyanto, H., & Nurushofa, F. A. (2024). Preparation CaO/MgO/Fe_3O_4 magnetite catalyst and catalytic test for biodiesel production. Results in Engineering, 22, 102202. https://doi.org/10.1016/j.rineng.2024.102202

[22]. Yang, L., Jin, L., Wang, K., Xu, H., He, G., & Chen, H. (2023). Interface coupling induced built-in electric fields boost electrocatalytic oxygen evolution reaction over MOF@LDHs core-shell nanocones. Colloids and Surfaces a Physicochemical and Engineering Aspects, 672, 131720. https://doi.org/10.1016/j.colsurfa.2023.131720

[23]. Sarno, M., Senatore, A., Scarpa, D., & Cirillo, C. (2020). “Green” synthesis of nanocarbons for reduced friction and wear. Lubricants, 8(2), 13. https://doi.org/10.3390/lubricants8020013

[24]. Hossain, M. S., Jahan, S. A., & Ahmed, S. (2023). Crystallographic characterization of bio-waste material originated CaCO3, green-synthesized CaO and Ca(OH)2. Results in Chemistry, 5, 100822. https://doi.org/10.1016/j.rechem.2023.100822

[25]. Rokni, K., Mostafaei, M., Soufi, M. D., & Kahrizi, D. (2021). Microwave-assisted intensification of transesterification reaction for biodiesel production from camelina oil: Optimization by Box-Behnken Design. Bioresource Technology Reports, 17, 100928. https://doi.org/10.1016/j.biteb.2021.100928

[26]. Helmi, M., & Hemmati, A. (2021). Synthesis of magnetically solid base catalyst of NaOH/Chitosan-Fe_3O_4 for biodiesel production from waste cooking oil: Optimization, kinetics and thermodynamic studies. Energy Conversion and Management, 248, 114807. https://doi.org/10.1016/j.enconman.2021.114807

[27]. Safitri, B., Yohandini, H., Muharni, M., Salni, S., & Hariani, P. L. (2024). Synthesis of $NiFe_2O_4$ Magnetic Using Artocarpus altilis Leave Extract for Photocatalytic Degradation of Methylene Blue Dye and Antibacterial Applications. Jurnal Kimia Sains Dan Aplikasi, 27(8), 371–380. https://doi.org/10.14710/jksa.27.8.371-380

[28]. Milano, J., Ong, H. C., Masjuki, H., Silitonga, A., Chen, W., Kusumo, F., Dharma, S., & Sebayang, A. (2018). Optimization of biodiesel production by microwave irradiation-assisted transesterification for waste cooking oil-Calophyllum inophyllum oil via response surface methodology. Energy Conversion and Management, 158, 400–415. https://doi.org/10.1016/j.enconman.2017.12.027